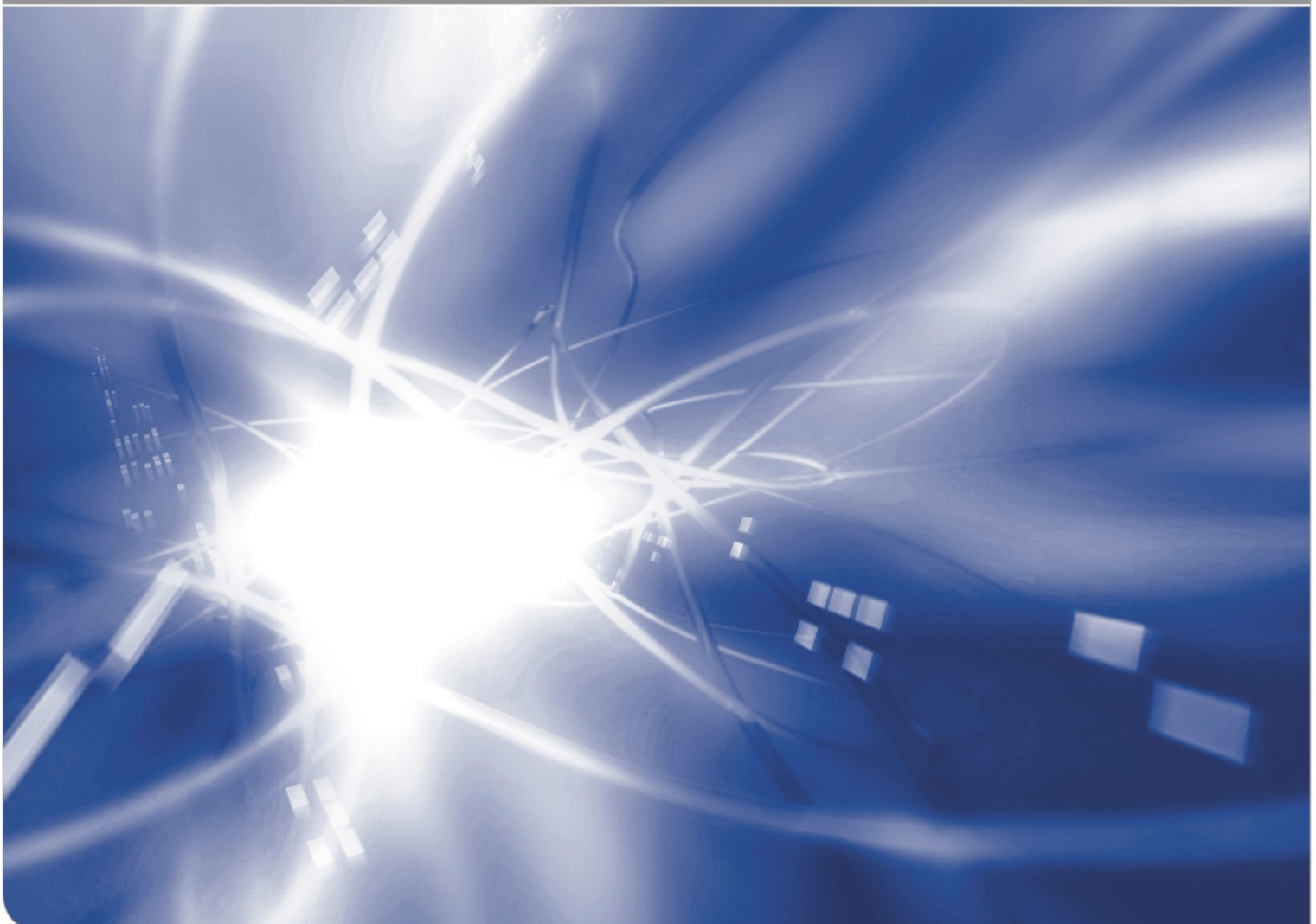


Stress-enhanced swelling of silica: Effect on residual deformation of bent fibers

T. Fett, G. Schell

KIT SCIENTIFIC WORKING PAPERS 79



Institut für Angewandte Materialien, Karlsruher Institut für Technologie (KIT)

Impressum

Karlsruher Institut für Technologie (KIT)
www.kit.edu



This document is licensed under the Creative Commons Attribution – Share Alike 4.0 International License (CC BY-SA 4.0): <https://creativecommons.org/licenses/by-sa/4.0/deed.en>

2018

ISSN: 2194-1629

Abstract

The deformation of water-affected silica fibers in 2-point-bending does not completely disappear after unloading. So far, this effect is discussed in literature as a stress relaxation at rather low temperatures. In the present study, we apply the swelling concept to the literature measurements. We found that the predictions of residual deformation via volume swelling by hydroxyl generation are in good agreement with the available experimental results.

Contents

1	Introduction	1
2	Equilibrium constant and hydroxyl content under stresses	1
3	Effect of swelling zones on bending deformation	2
4	Results	5
	4.1 Tests at 550°C	5
	4.2 Tests at 625 and 700°C	7
	4.3 Predictions including the effect of swelling stresses on diffusivity	8
5	Recovery of curvature after unloading	9
	References	11

1. Introduction

In the past, the authors showed in a couple of papers the principle effects of volume swelling by hydroxyl generation in silica on mechanics and fracture mechanics properties. Swelling of water-containing silica at high temperatures was early reported by Brückner [1,2], Shackelford [3] and Shelby [4]. An experimental proof of the swelling effect was given by deformation measurements on silica discs under 1-side soaking. The predicted and measured bending moments showed good agreement [5].

In most of our studies in the past, it was without importance what the effect of stress state on swelling is. We always could use *isotropic swelling* assuming identical strains in all directions. In [6] we applied the principle of Le Chatelier [7] for the computation of the equilibrium constant for water reaction with silica. This was done for non-isotropic stress states and allowed to predict the strength increase of silica fibers by swelling. We compared the predictions with strength measurements by Lezzi et al. [8]. Good agreement was found by using the results from Agarwal et al. [9] obtained with the Nuclear Resonance Analysis (NRA). In the actual note, we compare the swelling effect on residual bending displacements with deformation measurements by Tomozawa et al. [10].

2. Equilibrium constant and hydroxyl content under stresses

Water penetrated into silica reacts with the silica network according to



with the concentration of the hydroxyl $S = [\equiv\text{SiOH}]$ and that of the molecular water $C = [\text{H}_2\text{O}]$. For temperatures $>500^\circ\text{C}$, the equilibrium constant k of the reaction is

$$k = S^2 / C, \quad (2.2)$$

In [6] an equation was derived for the hydroxyl concentration as a function of stress. Following the procedure by Hamann [10], the equilibrium constant is given as:

$$RT \ln k = \mu_{0,\text{H}_2\text{O}} - 2\mu_{0,\text{SiOH}} + 2\Delta W + 2\Delta U, \quad k = S^2 / C, \quad (2.3)$$

where $\mu_{0,\text{H}_2\text{O}}$ and $\mu_{0,\text{SiOH}}$ are the chemical potentials for molecular water and hydroxyls, respectively in the unstressed state; ΔW represents the work per mol of SiOH in the volume V_0 done by the mechanical stresses. ΔU is the change of the elastic strain energy per mol due to a reduction of material stiffness because of the water reaction. The contribution ΔW is for uniaxial loading by $\sigma_z = \sigma_{\text{appl}}$

$$\Delta U / V_0 = -\frac{1}{2} \varepsilon_{\text{appl}}^2 \Delta E \quad (2.4)$$

where ΔE is the change in the Young's modulus as a consequence of the applied stresses. Due to the reaction between water and silica, a stiffness reduction of the SiO₂-structure, $\Delta E/\Delta S$, as can be concluded from sound velocity measurements in silica [11,12] with different hydroxyl content [13].

Since $\Delta E \leq 0$, the contribution ΔU has the same sign as ΔW . In the previous evaluations [6], the energy term, ΔU , was neglected and the undamaged Young's modulus was used in all equations. In this way, the computations yielded to *lower limit solutions*.

The derivation in [6] showed that the hydroxyl concentration is given as a function of the externally applied stress σ_{appl} in implicit form

$$S = S_0 \exp\left[(\sigma_{\text{appl}} + \beta S) \frac{\lambda}{RT}\right], \quad (2.5)$$

with the coefficient β that reflects the effect of swelling stresses on the equilibrium concentration due to the fact that the swelling stresses σ_{sw} are proportional to the swelling strains ε_v and these are proportional to the hydroxyl concentration S , i.e. $\sigma_{\text{sw}} \propto \varepsilon_v \propto S$. For *uniaxial loading*, σ_{appl} is the externally applied stress in axial direction, R the gas constant and T the absolute temperature and the parameter $\beta = -135$ GPa as derived in [6]. S_0 is the hydroxyl concentration in the absence of any stress.

The parameter λ was concluded from the bending experiments by Agarwal et al. [9]. By the evaluation in [6] it holds

$$\lambda = 14.4 \text{ cm}^3/\text{mol} \pm 10\% \quad (2.6)$$

Eq.(2.5) is an implicit equation since S occurs also in the exponential term. The explicit solution of (2.5) with respect to S reads

$$S = -\frac{RT}{\lambda \beta} \text{PLog}\left[-\frac{\lambda \beta S_0}{RT} \exp\left(\frac{\sigma_{\text{appl}} \lambda}{RT}\right)\right] \quad (2.7)$$

using the *product logarithm* or Lambert W function PLog , i.e. the solution $W = \text{PLog}(z)$ of the equation $z = W \exp(W)$ (see e.g. [14]).

The swelling stress in axial direction is according to [6]

$$\sigma_{\text{sw},z} \cong -133 \times S \quad (\text{GPa}) \quad (2.8)$$

3. Effect of swelling zones on bending deformation

Volume expansion under tensile loading must have consequences on the deformation behaviour, similar to the strength behaviour discussed in [6].

Under bending load, the effect of stress on the SiO₂/water reaction (2.1) is stronger in the tensile region than in the compression region. The enhanced swelling under tension

and suppressed swelling under compression zone must result in internal bending moment acting against the applied one.

In order to give a transparent analysis, let us consider a thin bent fiber of radius r_0 , Fig. 1a, loaded by a constant displacement of the fiber ends, Fig. 1b, and a constant force F , Fig. 1c. This fiber is water-vapour soaked under the externally applied outer fiber bending stress σ_b .

As long as the thickness of the water diffusion zone is small compared to the fibre radius, $b \ll r_0$, the bending stress in the diffusion zones is sufficiently constant. The applied stress at the surface as a function of the angle φ is given by

$$\sigma_{appl} = \sigma_b \cos \varphi \quad (3.1)$$

The thickness b of the diffusion and swelling layer is governed by diffusivity D and time t via

$$b = \sqrt{Dt} \quad (3.2)$$

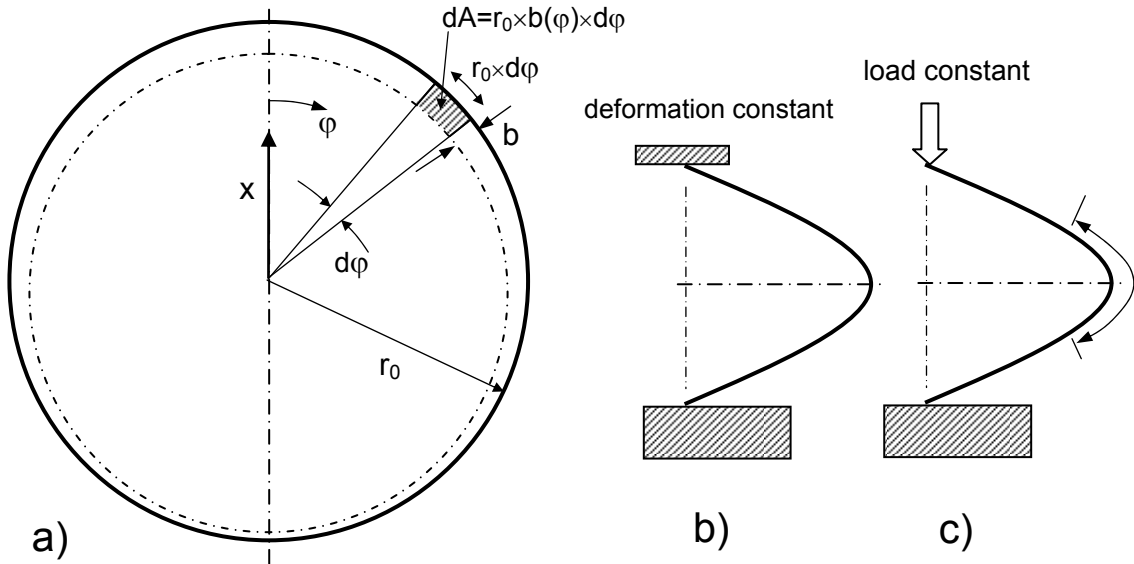


Fig. 1 a) Fiber cross-section with swelling zone under bending, b) bending under constant displacements at the ends, c) constant load (arrows indicate where water vapor acts).

The diffusivity to be used in eq.(3.2) is a function of stresses, commonly expressed by the hydrostatic stress component σ_h . When D_0 denotes its value in the absence of any stresses, the diffusivity for the case of stress-enhanced diffusion reads [15]

$$D = D_0 \exp \left[\frac{1}{3} \sigma_{appl} \frac{\Delta V_w}{RT} \right] \quad (3.3)$$

We used $\Delta V_w \approx 18 \text{ cm}^3/\text{mol}$ as was suggested in [8]. For thin diffusion layers the bending moment M_{sw} , caused by swelling stresses is

$$M_{sw} = \int_0^{2\pi} \sigma_{sw}(\varphi) b r_0 \cos \varphi dA \quad (3.4)$$

with the area element dA given by the hatched area in Fig. 1a

$$dA = r_0 b(\varphi) d\varphi \quad (3.5)$$

The eq.(3.4) can therefore be written

$$M_{sw} = r_0^2 \int_0^{2\pi} \sigma_{sw}(\varphi) b(\varphi) \cos \varphi d\varphi \quad (3.4a)$$

When the swelling zone becomes comparable with the fiber radius, e.g. $b > r_0/5$, the moment has to be computed by

$$M_{sw} = \int_{\varphi=0}^{2\pi} \int_{r=0}^{r_0} \sigma_{sw}(\varphi) (r \cos \varphi) r dr d\varphi \quad (3.4b)$$

After unloading the internal swelling moment M_{sw} causes a remaining curvature of

$$\frac{1}{R} = -\frac{M_{sw}}{EJ}, \quad J = \frac{\pi}{4} r_0^4 \quad (3.6)$$

Equation (3.4) gives the bending moment by swelling for the case of very thin swelling zones with $b/r_0 \rightarrow 0$. For thicker zones, comparable with the fiber radius r_0 , the solution becomes more complicated since then also the equilibrium conditions have to be fulfilled.

Because of the Bernoulli hypothesis that plane cross sections must remain plane, the fiber curvature caused by swelling results in a linear strain distribution over the cross section:

$$\varepsilon_z = c_1 x + c_2, \quad x = r \cos \varphi \quad (3.7)$$

(for x see Fig. 1a).

The integrals of swelling stresses over the cross section of the fiber allow consideration of different types of tests. The requirements of disappearing normal force of swelling stresses and disappearing total moment result in two conditions from which the unknown coefficients c_1 and c_2 can be determined

$$\int_{(A)} \left(\frac{1}{E} \sigma_{sw} + \beta x + \gamma \right) dA' = 0 \quad (3.8)$$

$$\int_A \left(\frac{1}{E} \sigma_{sw} + \beta x + \gamma \right) x dA' = 0 \quad (3.9)$$

For constant load, the equations (3.8) and (3.9) have to be solved simultaneously. For this purpose we used the *Mathematica* [16] subroutine *FindRoot*. Boundary conditions for constant displacement are realized by setting $c_1=0$.

Consequently, the eq.(2.7) now reads

$$S = -\frac{RT}{\lambda\beta} \text{PLog} \left[-\frac{\lambda\beta S_0}{RT} \exp \left(\frac{(\sigma_{\text{appl}} + Ec_2 + Ec_1 r \cos \varphi)\lambda}{RT} \right) \right] \quad (3.10)$$

4 Results

4.1 Tests at 550°C

Figure 2a shows the hydroxyl concentration at a water vapor pressure of 355 Torr as a function of temperature as reported by Davis and Tomozawa [17]. The data from IR-analyses are indicated by the circles. The right ordinate shows the hydroxyl concentration normalized on the value at 650°C.

At 550°C we can conclude that the ratio $S_{550^\circ\text{C}}/S_{650^\circ\text{C}}$ is about 1.4. The values of S_0 expected from the NR-Analysis [9, 6] are compiled in Table 1 for temperatures $\geq 550^\circ\text{C}$. For the parameter λ we tentatively used the 650°C result of $\lambda=14.4 \text{ cm}^3/\text{mol}$ also at 550°C, 625°C and 700°C.

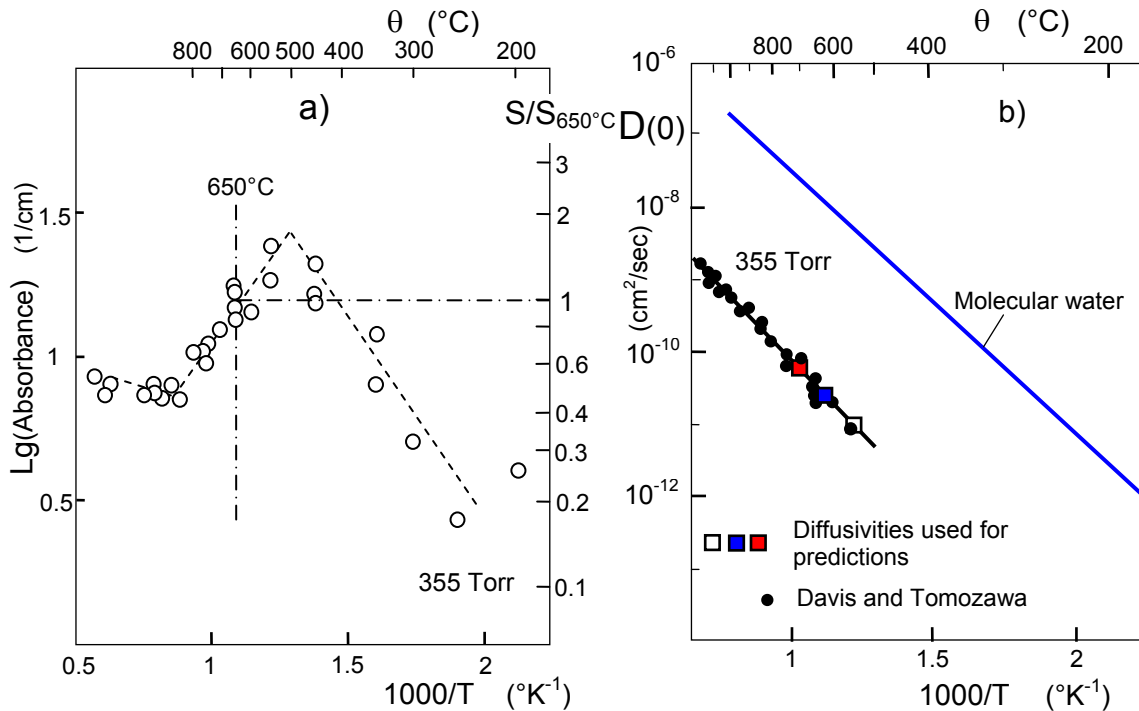


Fig. 2 a) Hydroxyl surface concentration S in silica, reported by Davis and Tomozawa [17] for a water vapor pressure of $p=355$ Torr (circles); right ordinate represents hydroxyl concentration S normalized on the concentration at reference temperature 650°C, $S_{650^\circ\text{C}}$; b) Diffusivity from literature [17] (circles); Squares: D_0 used for computations.

		NRA	NRA	$D(0)$
Temperature	$S/S_{650^\circ\text{C}}$	$S(0)$ (wt%)	S_0 (wt%)	(cm^2/s)
650°C (via NR-data)	1	0.586	0.652	
550°C	1.4	0.821	0.971	1×10^{-11}
625°C	1.07	0.63	0.71	3×10^{-11}
700°C	0.87	0.51	0.56	7×10^{-11}

Table 1: Hydroxyl concentrations from NRA-measurements used for the deformation predictions according to [9, 6, 17].

The effect of the different loading conditions is shown in Fig. 3a. Since in 2-point-bending tests the bending moment changes along the fibre length axis and due to the fact that the water reaction only took place in a central region (indicated by the arrows in Fig. 1c), no well-defined mechanical boundary conditions are given. As limit case, we consider constant moment and constant curvature.

In Fig. 3 computations are shown that are performed for a bending stress of 493 MPa at 355 Torr vapour pressure and a diffusivity of $D_0 = 1 \times 10^{-11} \text{ cm}^2/\text{s}$ as indicated by the open square in Fig. 2b. Under constant load ($\beta \neq 0, \gamma \neq 0$) the dash-dotted line resulted and for constant displacement ($\beta = 0, \gamma \neq 0$), the solid curve was obtained. The circles represent the experimental data from [10].

The effect of the applied bending stress is visible from Fig. 3b. The results agree sufficiently with the experimental data from [10] for all applied bending stresses. The perpendicular lines indicate upper limit for the time range in which the swelling layer thickness is smaller than $b = 10 \mu\text{m}$.

It is self-evident that the residual curvatures cannot increase unlimited with time. For long times the diffused water has homogeneously soaked the full cross section, i.e. $S_0 = \text{const}$. The saturation moment results then from eq.(3.4b).

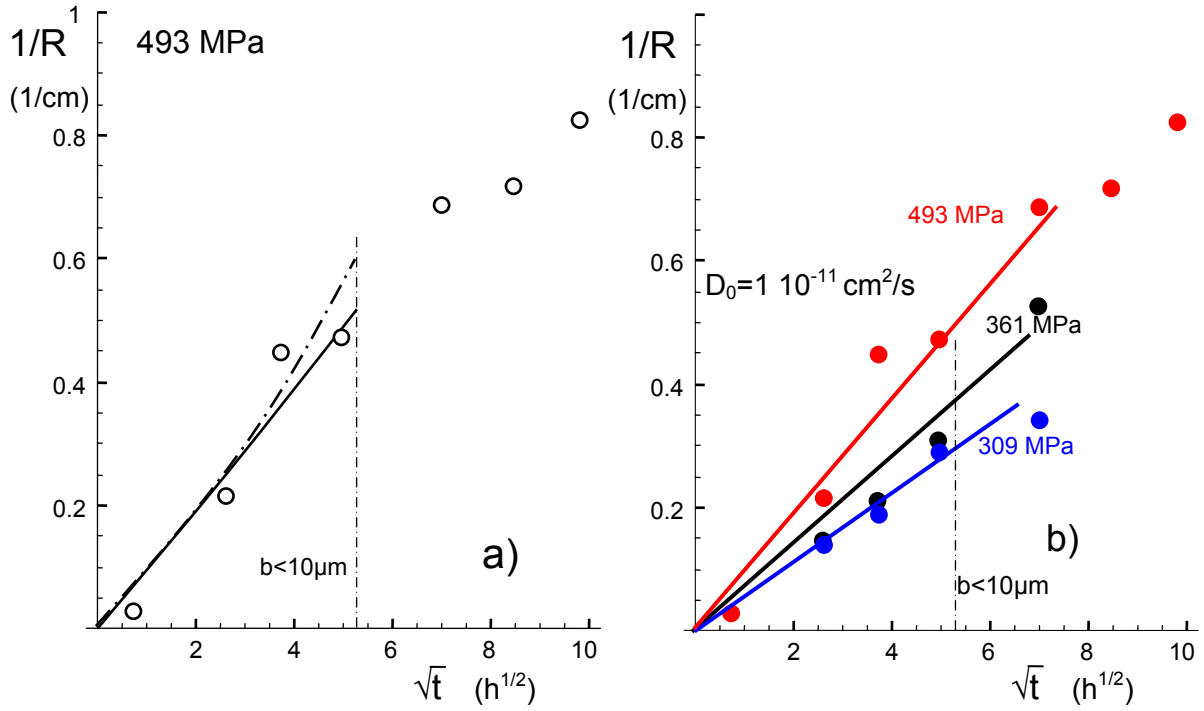


Fig. 3 Residual curvature of water vapour soaked silica fibers (125 μm diameter). Comparison of experimental results at different bending stresses with theoretical predictions; circles: results obtained in constant displacement tests, reported by Tomozawa et al. [10]. a) Effect of different boundary conditions: Bending tests by Tomozawa et al. [10] given by the circles, solid curve: constant displacement (Fig. 1b), dash-dotted curve: constant load (Fig. 1c); b) computation for different loads.

4.2 Tests at 625 and 700°C

Residual deformations were also measured at increased temperatures [10]. In addition to the results at 550°C (circles), Fig. 4 represents the data for 625°C (squares) and 700°C (triangles), all at 493 MPa. The diffusivities for computations are about $D_0=3 \cdot 10^{-11} \text{cm}^2/\text{s}$ at 625°C (blue square in Fig. 2b) and $D_0=7 \cdot 10^{-11} \text{cm}^2/\text{s}$ at 700°C (red square in Fig. 2b). The hydroxyl concentration at 625°C is about 7% higher than at 650°C: $S_{0,625^\circ\text{C}} \cong 1.13\%$ and at 700°C about 15% smaller: $S_{0,700^\circ\text{C}} \cong 0.92 \text{ wt}\%$.

The solid lines in Fig. 4 represent the computations. Whereas for 550°C a good agreement between measurement and computations is visible, at higher temperatures of 625° and 700°C the measurements are clearly underestimated by the computations.

At 625°C the predictions are 75% and at 700°C about 55% of the measured values. By varying the diffusivities D_0 , the computations were matched to the experimental data as shown by the dashed curves. The diffusivities obtained via curve fitting are introduced in Fig. 5 by the squares.

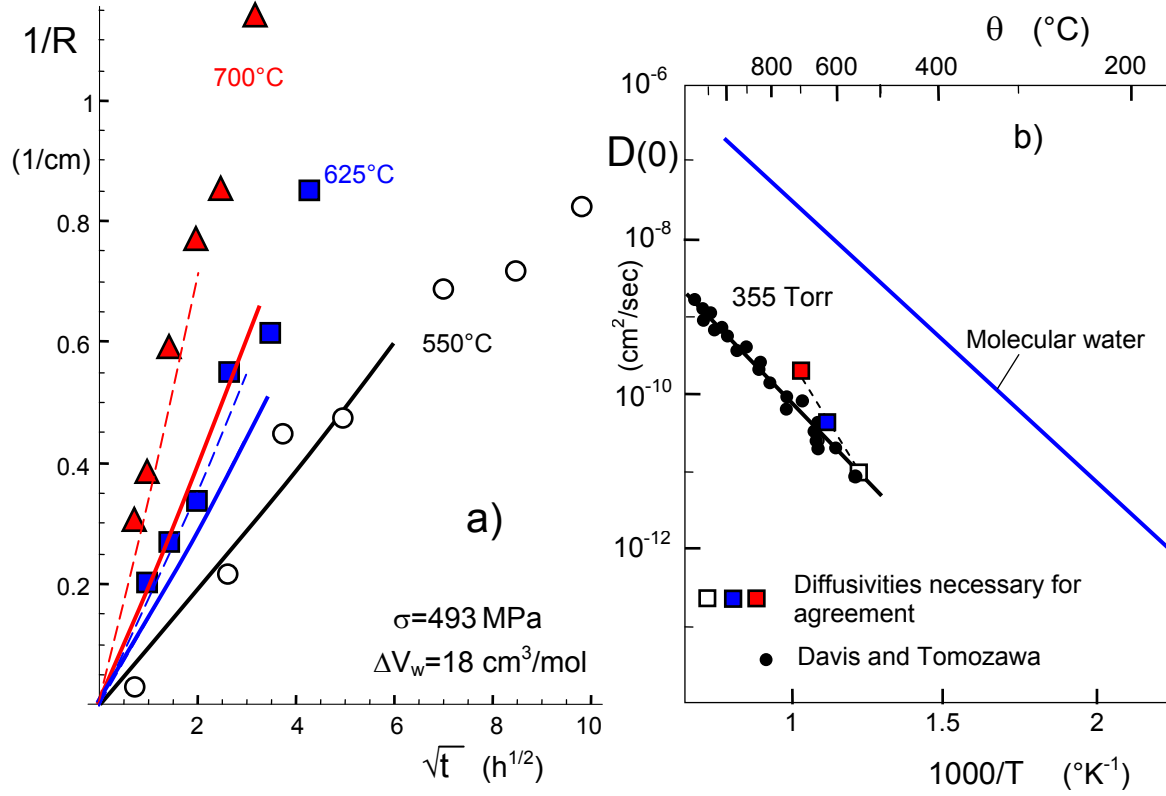


Fig. 4 Residual curvatures at different temperatures (NRA-data used). Symbols: Measurements by Tomozawa et al. [10], solid curves: computations using the diffusivities from Fig. 2b, dashed curves: Diffusivities matched to the measurements; b) Diffusivities giving best agreement with the measured curvatures.

4.3 Predictions including the effect of swelling stresses on diffusivity

The predictions made in Section 4.2 were performed with eq.(3.3) that implicitly assumes that the stresses acting in a volume element would be externally applied stresses exclusively. In presence of swelling stresses, this equation must read

$$D = D_0 \exp \left[(\sigma_{h,appl} + \sigma_{h,sw}) \frac{\Delta V_w}{RT} \right] \quad (4.1)$$

The hydrostatic swelling stress term for *anisotropic swelling*, $\alpha=1.92$, reads according to [6]

$$\sigma_{h,sw} = \frac{1}{3}(\sigma_{sw,z} + \sigma_{sw,y}) = -\frac{\kappa E}{6(1-\nu)}(1 + \alpha)S \cong -41 \text{ GPa} \times S \quad (4.2)$$

and for isotropic swelling with $\alpha=1/3$ to be applied in the computation of D_0 from $D(0)$ for the unloaded case, $\sigma_{appl}=0$,

$$\sigma_{h,sw} = -\frac{2\kappa E}{9(1-\nu)}S \cong -18.7 \text{ GPa} \times S \quad (4.3)$$

This implies for the unknown diffusivity D_0 in the absence of any stress:

$$D_0 = D(0) \exp \left[18.7 (\text{GPa}) \times S_0 \frac{\Delta V_w}{RT} \right] \quad (4.4)$$

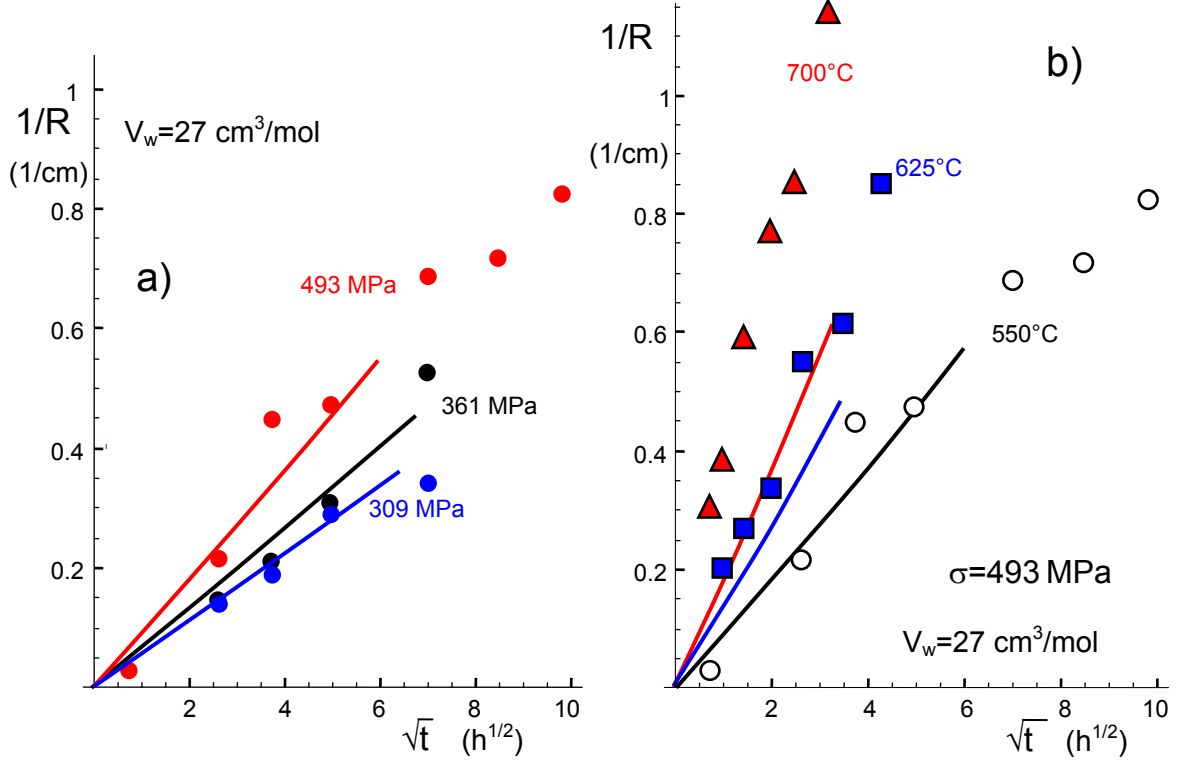


Fig. 5 a) Curve fitting according to (4.1) for $\theta=550^\circ\text{C}$, resulting in $\Delta V_w=27 \text{ cm}^3/\text{mol}$, b) predictions for temperatures of 625°C , and 700°C .

We varied the volume ΔV_w and computed the residual curvatures for the three stresses at 550°C and compared the results with the measurements by using the *Mathematica* Subroutine *NonlinearFit* [16]. The best parameter set was found by matching the computed curves to the measured data by Tomozawa et al. [10] as $\Delta V_w=27 \text{ cm}^3/\text{mol}$. The related set of curves is shown in Fig. 5a. Application to the higher temperatures again underestimates the measurements as is visible from Fig. 5b.

5. Recovery of curvature after unloading

The hydroxyl concentration at the end of a bending test ($\sigma_{\text{bend}} = 493 \text{ MPa}$, $t = 36 \text{ h}$) is shown in Fig. 6a as the red curve. The S -distribution is non-symmetric with respect to the centreline. On the tensile side, the concentration S is enhanced due to the tensile stresses and on the compression side reduced. The hydroxyl profile in the absence of externally applied stresses is represented by the black curve. This curve is of course symmetric.

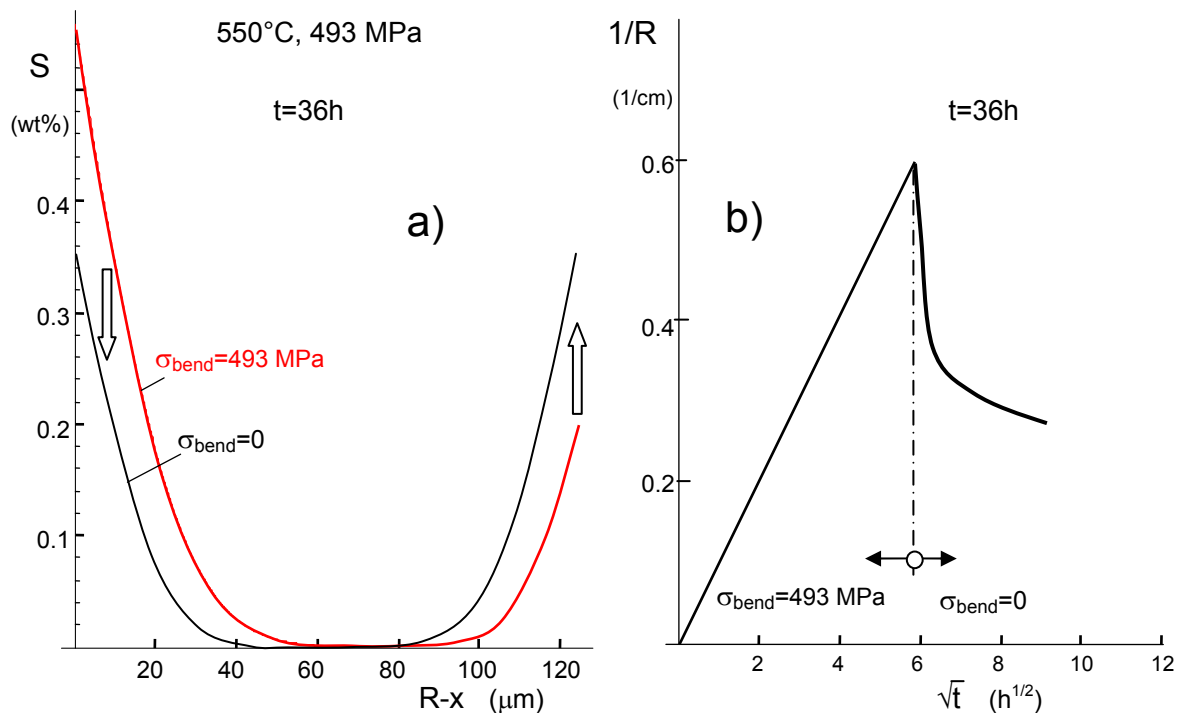


Fig 6 a) Hydroxyl concentration along the diameter of a bent fiber (red curve) compared with the S profile in the absence of bending, b) expected mechanical response of curvature for changes in the equilibrium constant and hydroxyl concentration.

If the bent fiber is unloaded and cooled down to room temperature, the S -distribution remains unchanged, and the S -profile caused by bending is “frozen in”. No time-dependent “recovery” of the residual curvature is possible.

When the fiber is unloaded at the soaking temperature, the equilibrium constant must decrease because it is no longer stress-enhanced. The consequence is that the equilibrium of the reaction (2.1) tends more to the left side generating molecular water. The downward arrow in the former tensile region indicates this. The time necessary for the reaction can be rather short since diffusion processes are not necessary and generated molecular water can reside in the holes of the silica network. In the compression region, the equilibrium constant must increase and, consequently, the S -concentration (indicated by an arrow upwards). This reaction is expected to be slowly since the additional water must diffuse from the surface.

The changes in S -concentration cause changes in volumetric strains. Changes in swelling strains give rise for a change in swelling stresses. In the former tensile region, the swelling stresses decrease and in the former compression region, swelling stresses increase. The mechanical response is a time-dependent reduction of the curvature as schematically illustrated in Fig. 6b. This type of a “relaxation” or better “recovery” is of course only a consequence of an increase or decrease in S with time.

References

- 1 Brückner, R., “The structure-modifying influence of the hydroxyl content of vitreous silicas,” *Glastech. Ber.* **43**(1970), 8-12.
- 2 Brückner, R., “Metastable equilibrium density of hydroxyl-free synthetic vitreous silica,” *J. Non-Cryst. Solids*, **5**(1971), 281-5
- 3 Shackelford, J.F., Masaryk, J.S., Fulrath, R.M., “Water Content, Fictive Temperature and Density Relations for Fused Silica,” *J. Am. Ceram. Soc.* **53**(1970), 417.
- 4 Shelby, J.E., “Density of vitreous silica,” *J. Non-Cryst.* **349** (2004), 331-336.
- 5 S. M. Wiederhorn, F. Yi, D. LaVan, T. Fett, M.J. Hoffmann, Volume Expansion caused by Water Penetration into Silica Glass, *J. Am. Ceram. Soc.* **98**(2015), 78-87.
- 6 S. M. Wiederhorn, G. Rizzi, S. Wagner, M. J. Hoffmann, and T. Fett, Stress-Enhanced Swelling of Silica: Effect on Strength, *J. Am. Ceram. Soc.* **99**(2016), 2956-63.
- 7 H. Le Chatelier, *C.R. Acad. Sci. Paris* **99**(1884), 786
- 8 P.J. Lezzi, Q.R. Xiao, M. Tomozawa, T.A. Blanchet, C.R. Kurkjian, Strength increase of silica glass fibers by surface stress relaxation: A new mechanical strengthening method, *J. of Non-Crystalline Solids* **379** (2013) 95–106.
- 9 A. Agarwal, M. Tomozawa, W. A. Lanford, Effect of stress on water diffusion in silica glass at various temperatures, *J. Non-Cryst.* **167**(1994), 139-148.
- 10 M. Tomozawa, P.J. Lezzi, R.W. Hepburn, T. A. Blanchet, D. Cherniak, Surface Stress Relaxation and Resulting Residual Stress in Glass Fibers: A New Mechanical Strengthening Mechanism of Glasses, *J. Non-Cryst. Solids* **358**(2012), 2650.
- 11 D.B. Fraser, Factors Influencing the Acoustic Properties of Vitreous Silica, Citation: *Journal of Applied Physics* 39(1968), 5868-5878.
- 12 R Le Parc, C Levelut, J Pelous, V Martinez, B Champagnon, Influence of fictive temperature and composition of silica glass on anomalous elastic behavior *J. Phys.: Condens. Matter* **18**(2006), 7507-27.
- 13 T. Fett, K. G. Schell, M. J. Hoffmann, and S. M. Wiederhorn, Effect of damage by hydroxyl generation on strength of silica fiber, under Review for *J. Am. Ceram. Soc.*
- 14 R. Corless, G. Gonnet, D. Hare, D. Jeffrey and D. Knuth, “On the Lambert W Function,” *Advances in Computational Mathematics*, **5**(1996), 329-359.
- 15 P.G. Shewman, *Diffusion in Solids*, McGraw-Hill, New York, 1963.
- 16 *Mathematica*, Wolfram Research, Champaign, USA.
- 17 Davis, K.M., Tomozawa, M., Water diffusion into silica glass: structural changes in silica glass and their effect on water solubility and diffusivity, *J. Non-Cryst. Sol.* **185**(1995), 203-220.

KIT Scientific Working Papers
ISSN 2194-1629

www.kit.edu